Bistable Resistive Switching of a Sputter-Deposited Cr-doped $SrZrO_3$ Memory Film

Chih-Yi Liu, Pei-Hsun Wu, Arthur Wang, Wen-Yueh Jang, Jien-Chen Young, Kuang-Yi Chiu, and Tseung-Yuen Tseng, *Fellow, IEEE*

***Abstract*—Sputter-deposited Cr-doped $SrZrO_3$-based metal–insulator–metal structures exhibited bistable resistive reversible switching as observed under bias voltage and voltage pulse. The ratio of resistance of the two leakage states (high-H, low-L) was about five orders of magnitude. The conduction of the L-state satisfied Frenkel–Poole emission and that of the H-state followed ohmic mechanism, causing the resistance ratio to decrease with increasing bias voltage. The transition time of H- to L-state was five orders of magnitude higher than that of L- to H-state. The transition from H- to L-state was the restricted part for reversible switching operation. The difference in transition time of the two states should be related to the respective conduction mechanisms.**

***Index Terms*—Conduction mechanism, nonvolatile memory, resistive switching memory, $SrZrO_3$.**

I. Introduction

PEROVSKITE materials have been widely investigated for many applications, such as dynamic random access memory, superconductor, and gate oxide for CMOS [1]–[3]. Recently, the Cr-doped perovskite films have been investigated by Beck *et al.* for nonvolatile memory application, which is called as resistance random access memory (RRAM) [4]–[6]. The RRAM with the properties of the reversible switching between the low (L) and the high (H) leakage states, and the multilevel switching is a promising candidate for nonvolatile memory application. However, so far the reasons for the resistive switching induced by voltage pulse or bias voltage are not clear. In this letter, the sputter method is used for the first time to fabricate the Cr-doped $SrZrO_3$-based metal–insulator–metal (MIM) structure and the conduction mechanisms of the device are investigated. The deposition method, the substrate, the electrode materials, and process temperature were adopted for low cost and integration considerations. The resistive transitions between the two leakage states are also changed by voltage pulse. The different transition times for the switching between the two leakage states are indicated for the first time.

Manuscript received January 3, 2005; revised March 3, 2005. This work was supported in part by the National Science Council, Taiwan, R.O.C., under Project NSC 92-2215-E009-016 and in part by the Winbond Electronics Corporation, Taiwan, R.O.C. The review of this letter was arranged by Editor C.-P. Chang.

C.-Y. Liu, P.-H. Wu, and T.-Y. Tseng are with the Department of Electronics Engineering and Institute of Electronics, National Chiao-Tung University, Hsinchu 300, Taiwan, R.O.C.

A. Wang, W.-Y. Jang, J.-C. Young, and K.-Y. Chiu are with Winbond Electronics Corporation, Hsinchu 300, Taiwan, R.O.C. (e-mail: tseng@cc.nctu.edu.tw).

Digital Object Identifier 10.1109/LED.2005.848073

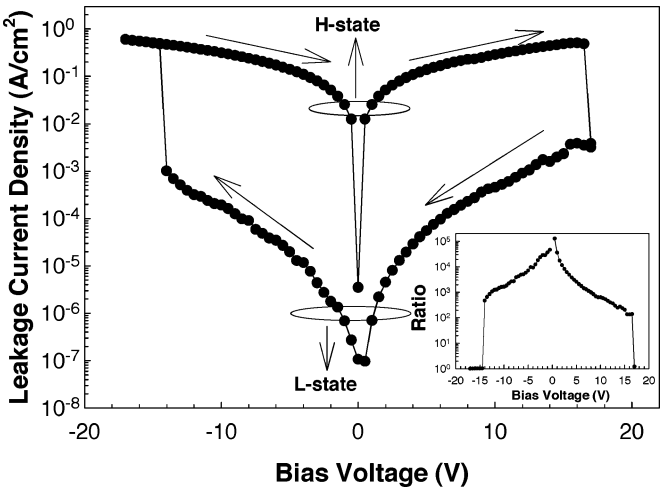

Fig. 1. Leakage current density versus bias voltage for Cr-doped $SrZrO_3$-based MIM device. The inset shows the variation of the resistance ratio with the bias voltage.

II. Experimental

A 200-nm SiO_2 layer was thermally grown on Si substrate in a furnace to prevent the leakage current from the Si substrate. A 50-nm $SrTiO_3$ buffer layer and then a 60-nm $LaNiO_3$ (LNO) bottom electrode film were deposited by radio frequency (RF) magnetron sputter on the SiO_2–Si substrate. Subsequently, a 90-nm 0.2% Cr-doped $SrZrO_3$ (SZO) film was deposited at 450 °C by RF magnetron sputter on LNO film as an insulator layer. The SZO film exhibits the (100), (110), and (200) peaks based on X-ray diffraction pattern (not shown here), indicating that it is polycrystalline structure. Finally, a 500-nm-thick Al film was deposited by thermal evaporation on the Cr-doped SZO films as a patterned top electrode of area 4.9×10^{-4} cm^2 to perform the electrical measurement with Agilent 4155C and 81 110A.

III. Results and Discussion

Fig. 1 shows the leakage current density versus bias voltage for the 0.2% Cr-doped SZO-based MIM device. The reproducible sequence of leakage current density can be traced from an increase of leakage current density for the high leakage (H) state with increasing bias voltage in the positive direction. At 15 V, the leakage current density rapidly decreased from H to low leakage (L) state. The leakage current density of the L-state increased with increasing bias voltage in the negative direction and rapidly increased from L to H state at −15 V. The switching voltage should relate to the crystallinity of the resistive film.

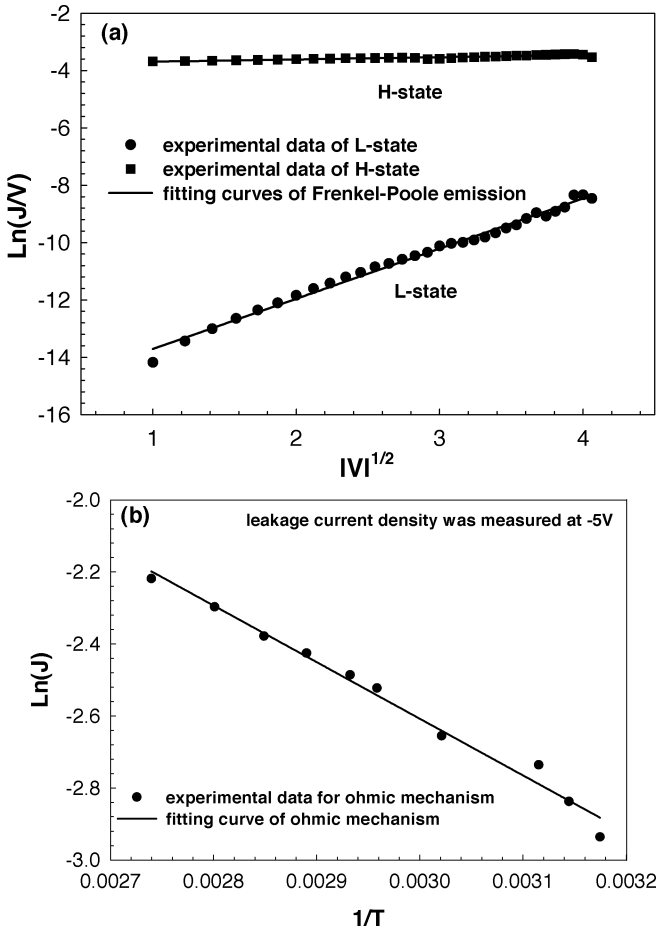

Fig. 2. (a) Ln(J/V) versus $|\mathrm{V}|^{1/2}$ for the high and the low leakage states. (b) Ln(J) versus 1/T for the high leakage state.

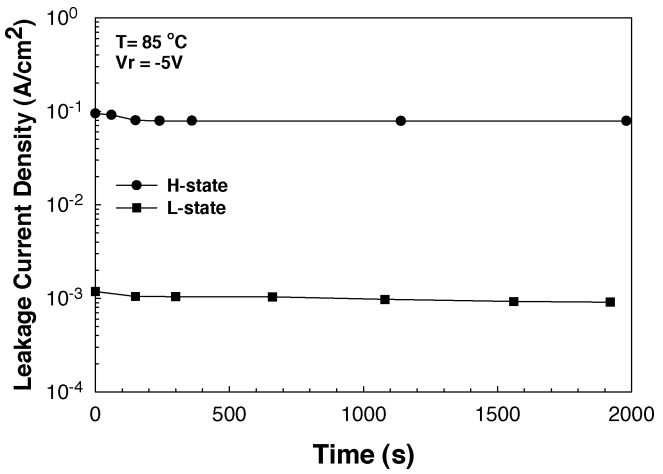

Fig. 3. Variation of the leakage current density with time at 85 °C for the high and the low leakage states.

The polarity direction of resistive transition is an intrinsic property for the device. The inset of Fig. 1 shows the resistance ratio that decreased with increasing voltage in both directions (10^5 at a low voltage and 10^3 at 10 V) for the two leakage states. As so far this is the biggest resistance ratio for SZO material. The large resistance ratio can provide enough margins to separate the different memory states. The same trend in the ratio under either direction indicates the identical influence of the resistive transition. Furthermore, the different dopant concentrations in SZO material were also investigated. While the dopant concentration was twice larger or less than the 0.2% Cr concentration, the resistive change properties were worse or disappeared. From the band diagram of the MIM structure, which has a configuration of Al–Cr-doped SZO/LNO, one can know that the carrier sources of leakage current under positive and negative bias voltage originate from different directions. Because of the different electrode materials and process sequence, the bottom and top interface layers should be quite different and the responses of the bottom and top interface layers for the resistance transition should be different. Therefore, the similar trend in the leakage current density variation and the resistance ratio in the both directions after the resistive transition should be resulted from the effect of Cr-doped SZO film, not from that of the interface layers. Fig. 2(a) depicts the plots of Ln(J/V) versus $|\mathrm{V}|^{1/2}$ for the H- and L-states. The L-state conduction follows Frenkel–Poole emission as indicated by a good linear fit to the experimental data [7]. The Frenkel–Poole emission is due to field-enhanced thermal excitation of trapped electrons into the conduction band. The near zero slope of the linear fit for H-state indicates that Frenkel–Poole emission is not the dominated mechanism and implies that the ohmic mechanism is the possible conduction mechanism for the H-state. The plot of Ln(J) versus 1/T in Fig. 2(b) indicates that ohmic mechanism is indeed responsible for the H-state [7]. The leakage current density owing to ohmic conduction is related to thermal excited electrons hopping from one isolated state to the next. There are some nonlinearity in the fitting capacitance–voltage (*I–V*) curves shown in Fig. 2(a) and (b), which possibly caused by the contribution of two or more conduction mechanisms, measurement noise, or nonideal condition. Therefore, we use dominated mechanism for explaining the conduction of H- and L-states. Furthermore, the Cr dopant should also play an important role in the ohmic mechanism. Therefore, the leakage current density of L-state increased in accordance with $V_{\exp}(V^{1/2})$ and that of H-state increased linearly with increasing bias voltage. So the resistance ratio of the two leakage states decreased with increasing bias voltage (inset of Fig. 1). The conduction mechanisms of the both leakage states were all bulk controlled, not interface controlled. The results are consistent with the previous discussion about the resistive transition. A retention time of more than 1800 s at 85 °C was obtained for the Cr-doped MIM device (Fig. 3), indicating that the device with such a long retention characteristic. Furthermore, the device with the properties of reversible switching and nondestructive readout can serve as a nonvolatile memory device. Fig. 4(a) shows the variation of leakage current density as a function of bias voltage of the device and the response of the device after applying a -20 V, 5 ns pulse on the top electrode. That is, applying a negative voltage pulse on the device changed the L-state to H-state. On the other hand, Fig. 4(b) shows the switching of the H-state to the L-state after applying a 20-V, 500 μs pulse. The influence of pulse amplitude on the resistance change was also investigated (not shown here). While the positive pulsewidth was larger than 500 μs and the negative one was larger 5 ns, the pulse amplitude larger than the switching voltage of dc voltage

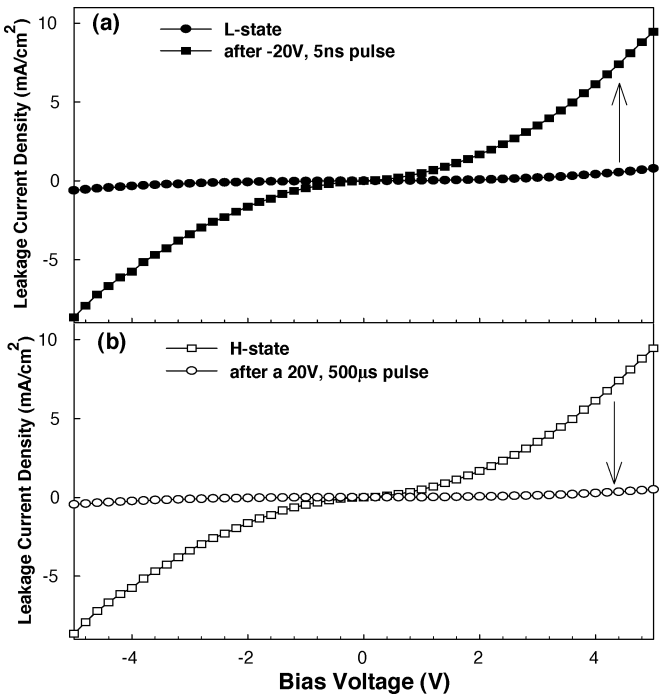

Fig. 4. (a) Leakage current density versus bias voltage for low leakage state and (b) for high leakage state after adding the voltage pulse indicated.

sweep would change the state to the other state. The resistance change driven by the voltage pulses had the same polarity direction with that driven by the bias voltages. We have made the same fitting as Fig. 2 using the data in Fig. 4 (not shown here). It is indicated that the conduction mechanism of L-state is dominated by Frenkel–Poole emission. Furthermore, it was found that the conduction mechanism of H-state is related to Frenkel–Poole emission under low bias voltage while under high bias voltage, the conduction of H-state is still governed by ohmic mechanism. This phenomenon may be attributed to that the pulse operation has smaller transition time than the dc voltage sweep. The transition time for the switching of the H- to the L-state was five orders of magnitude longer than that of L- to H-state, implying that the transition from L- to H-state was easier than from H- to L-state. Therefore, the transition from H- to L-state is the restricted part for the reversible switching by voltage pulse operation.

IV. Conclusion

Cr-doped SZO films were deposited by RF magnetron sputter to fabricate the MIM device under investigation. This device with the properties of reversible switching, nondestructive readout, and a long memory time is suitable for nonvolatile memory application. The conduction mechanisms corresponding to H- and L-states were investigated to provide some explanations for resistive transition. The resistance transition could also be driven by voltage pulses. The transition time of H- to L-state was five orders of magnitude longer than that of L- to H-state.

References

[1] M. S. Tsai, S. C. Sun, and T. Y. Tseng, "Effect of bottom electrode materials and the electrical and reliability characteristics of (Ba, Sr) TiO_3 capacitors," *IEEE Trans. Electron Devices*, vol. 46, no. 12, pp. 1829–1838, Dec. 1999.

[2] C. J. Haung, C. Y. Chang, and T. Y. Tseng, "Bolometric response of superconducting $YBa_2Cu_3O_{7-x}$ microbridges," *J. Appl. Phys.*, vol. 72, pp. 5786–5791, 1992.

[3] C. Y. Liu, H. T. Lue, and T. Y. Tseng, "Effects of nitridation of silicon and repeated spike heating on the electrical properties of $SrTiO_3$ gate dielectrics," *Appl. Phys. Lett.*, vol. 81, pp. 4416–4418, 2002.

[4] A. Beck, J. G. Bednorz, C. Gerber, C. Rossel, and D. Widmer, "Reproducible switching effect in thin oxide films for memory applications," *Appl. Phys. Lett.*, vol. 77, pp. 139–141, 2000.

[5] Y. Watanabe, J. G. Bednorz, A. Bietsch, C. Gerber, D. Widmer, A. Beck, and S. J. Wind, "Current-driven insulator-conductor transition and nonvolatile memory in chromium-doped $SrTiO_3$ single crystals," *Appl. Phys. Lett.*, vol. 78, pp. 3738–3740, 2001.

[6] C. Rossel, G. I. Meijer, D. Bremauid, and D. Widmer, "Electrical current distribution across a metal-insulator-metal structure during bistable switching," *J. Appl. Phys.*, vol. 90, pp. 2892–2898, 2001.

[7] S. M. Sze, *Physics of Semiconductor Device*, 2nd ed. New York: Wiley, 1981.